Hindawi
Cellular Microbiology
Volume 2022, Article ID 7647976, 17 pages
https://doi.org/10.1155/2022/7647976

Research Article

Plasmodium berghei-Mediated NRF2 Activation in Infected Hepatocytes Enhances Parasite Survival

Annina Bindschedler,[1,2] **Jacqueline Schmuckli-Maurer**,[1] **Rahel Wacker**,[1,2] **Nicolas Kramer**,[1] **Ruth Rehmann**,[1] **Reto Caldelari**,[1] **and Volker T. Heussler**[1]

[1]*Institute of Cell Biology, University of Bern, Bern, Switzerland*
[2]*Graduate School for Cellular and Biomedical Sciences, University of Bern, Bern, Switzerland*

Correspondence should be addressed to Volker T. Heussler; volker.heussler@unibe.ch

Received 17 December 2021; Accepted 16 February 2022; Published 12 March 2022

Academic Editor: Roberto Botelho

The protozoan parasite *Plasmodium*, causative agent of malaria, initially invades and develops in hepatocytes where it resides in a parasitophorous vacuole (PV). A single invaded parasite develops into thousands of daughter parasites. Survival of the host cell is crucial for successful completion of liver stage development. Nuclear factor erythroid-derived 2-related factor 2 (NRF2) is a transcription factor known to induce transcription of cytoprotective genes when activated. Here we show that NRF2 is activated in *Plasmodium berghei*-infected hepatocytes. We observed that this NRF2 activation depends on PV membrane resident p62 recruiting KEAP1, the negative regulator of NRF2. Disrupting the NRF2 gene results in reduced parasite survival, indicating that NRF2 signaling is an important event for parasite development in hepatocytes. Together, our observations uncovered a novel mechanism of how *Plasmodium* parasites ensure host cell survival during liver stage development.

1. Introduction

Malaria is caused by the protozoan parasite *Plasmodium*, which is transmitted by *Anopheles* mosquitoes. During a blood meal, an infected female *Anopheles* mosquito injects sporozoites into the skin of the vertebrate host [1, 2]. A proportion of the parasites reaches blood vessels allowing them a passive transport to the liver. There, *Plasmodium* actively invades hepatocytes by invaginating the host cell plasma membrane leading to the formation of a parasitophorous vacuole (PV) in which the parasite resides throughout liver stage development [3]. The PV membrane (PVM) acts as the main interface between the parasite and the host cell cytoplasm. It is considerably remodeled by the parasite through the export of parasite proteins [4]. PVM integrity is crucial for parasite survival and development. Within the PV, the parasite develops into a growing liver stage trophozoite and later undergoes multiple nuclear divisions to form a large schizont. Invagination of the parasite plasma membrane leads to the formation of single daughter parasites, called merozoites [5]. Towards the end of liver stage development, PVM rupture leads to the release of the merozoites into the host cell cytoplasm inducing an ordered cell death of the host cell. The merozoites are released into an adjacent blood vessel in merosomes that bud off from the dying host cell [6]. Eventually, merosomes burst releasing free merozoites, which infect red blood cells thus initiating the symptomatic blood stage infection.

It has been shown earlier that the presence of the parasite protects the host cell from apoptosis [7]. However, little is known about the signaling events underlying parasite-dependent apoptosis resistance in host cells.

Nuclear factor erythroid 2-related factor 2 (NRF2), a member of the Cap'n'Collar (CNC) family of basic leucine zipper transcription factors, mediates intrinsic resistance to oxidative stress and controls the adaptive responses to various environmental stressors. It binds to a cis-acting enhancer with a core nucleotide sequence of 5′-RTGACNNNGC-3′ that is known as the antioxidant response element (ARE) to control the basic and inducible

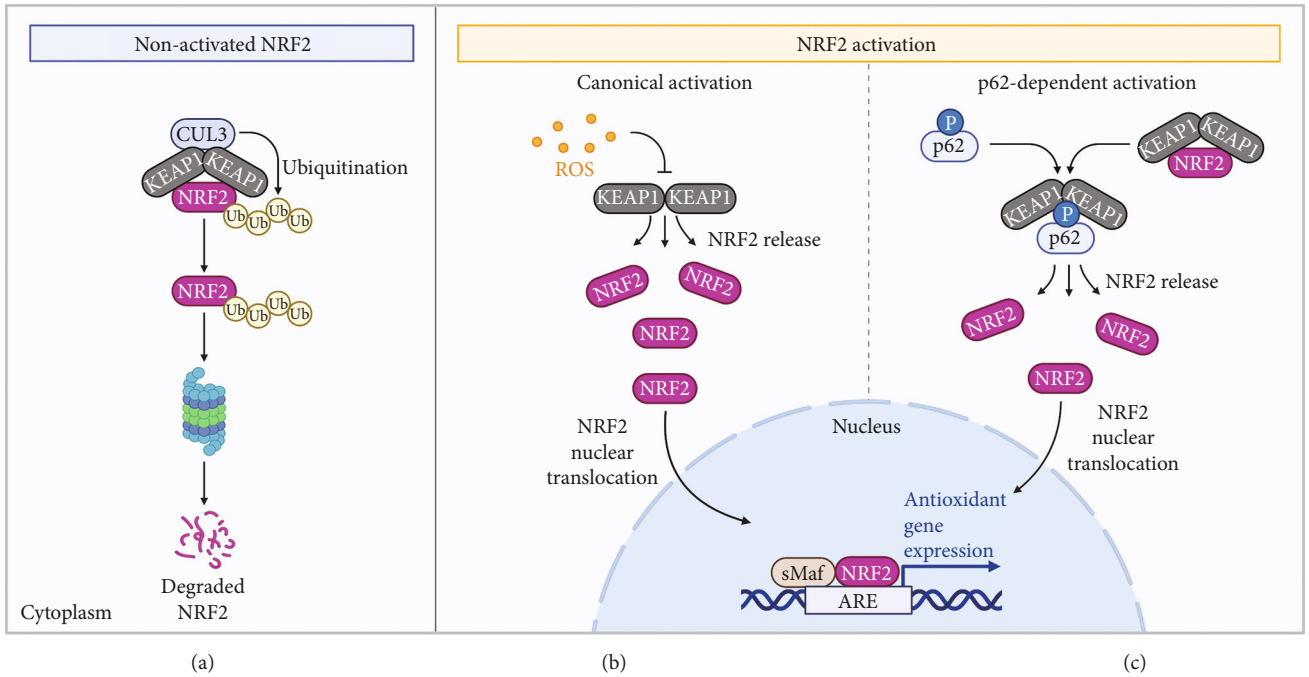

Figure 1: Canonical and p62-dependent NRF2 activation. (a) In nonstressed cells, NRF2 is constantly expressed and bound to its negative regulator KEAP1, which acts as an adaptor protein for the interaction with the E3 ubiquitin ligase CUL3. CUL3 constantly ubiquitinates NRF2 targeting it for proteasomal degradation. (b) Canonical activation: oxidation of cysteine residues in KEAP1 by reactive oxygen species (ROS) leads to a conformational change of the protein. In the oxidized state KEAP1 cannot bind to NRF2 anymore, leading to the release of NRF2. Free NRF2 translocates into the nucleus where it heterodimerizes with small Maf (sMaf) proteins and activates transcription of genes containing an antioxidant response element (ARE) in their regulatory region. (c) p62-Dependent activation: NRF2 protein stability can also be regulated through p62 competing with NRF2 for interaction with KEAP1. KEAP1 has a higher affinity for p62 phosphorylated at serine 349 than for NRF2, leading to the release and therefore activation of NRF2. Schematic adapted from "Keap1-Nrf2 Pathway," by BioRender.com (2021). Retrieved from https://app.biorender.com/biorender-templates.

expression of over a thousand genes. Target genes are involved in several cytoprotective pathways including detoxification response, heme metabolism, cell proliferation, and apoptotic resistance/survival regulation ([8–10]; [11, 12]). Importantly, several NRF2 target genes have recently been shown by single cell mRNA seq analysis to be upregulated upon *P. berghei* infection of hepatocytes [13]. Another transcriptome study in *P. vivax*-infected hepatocytes also identified NRF2 regulated expression as a pathway supporting parasite persistence suggesting an important and conserved function of this host cell transcription factor [14].

Under quiescent conditions, NRF2 is negatively regulated by Kelch-like ECH associated protein 1 (KEAP1), a redox-sensitive E3 ubiquitin ligase substrate adaptor [15]. KEAP1 binds to NRF2, mediating its ubiquitination through the E3 ubiquitin ligase Cullin3 (CUL3), leading to the degradation of NRF2 through the ubiquitin proteasome pathway ([16, 17]; [18]) (Figure 1(a)). In response to oxidative stress, oxidation of cysteine residues in KEAP1 leads to a change in conformation which releases NRF2 and therefore protects it from being degraded [19, 20]. Free NRF2 translocates to the nucleus where it heterodimerizes with members of the sMaf protein family and induces transcription of its target genes [21] (Figure 1(b)).

Besides this canonical pathway, NRF2 protein stability can also be influenced by p62/sequestosome-1 (hereafter referred to as p62). p62 plays a crucial role in selective autophagy where it ensures substrate selectivity by delivering polyubiquitinated cargo to LC3 (microtubule-associated protein 1 light chain 3)-positive autophagosomal membranes. However, p62 also functions in the NRF2 regulation by interacting with the NRF2 binding site of KEAP1 and competitively inhibiting the KEAP1-NRF2 interaction, leading to NRF2 stabilization and subsequent nuclear translocation [22–24] (Figure 1(c)). The binding affinity of KEAP1 for p62 is greatly enhanced by p62 phosphorylation at serine 349 [25]. Of note, p62 is itself a NRF2 target gene, thus creating a positive feedback loop [26].

Previously, we have shown that p62 is recruited to the *P. berghei* PVM by the autophagy marker protein LC3. However, the role of p62 at the PVM is not clear yet, since it does not seem to act in its classical function as selective autophagy receptor [27]. As p62 is involved in NRF2 and subsequent survival pathway activation, and it has been shown that the presence of the parasite protects the host cell from cell death, we sought to investigate the host cell NRF2 status in infected cells. Interestingly, we found that NRF2 is indeed activated in infected cells and that activation occurs mainly through p62. Furthermore, parasites developing in NRF2-deficient host cells showed significant reduction in survival. Altogether, we provide first evidence of the NRF2-signaling pathway contributing to *Plasmodium* survival during its liver stage development.

2. Results

2.1. NRF2 is Activated in Infected Cells. To investigate the activity of NRF2 in *Plasmodium*-infected cells we made use of a specific reporter, named OKD48 (KEAP1-dependent Oxidative stress Detector, No-48), which was developed by Oikawa et al. [28] and allows the monitoring of endogenous NRF2 activity. The OKD48 reporter consists of a luciferase cDNA (in our case a NanoLuc luciferase for maximum sensitivity) fused to a truncated version of NRF2 (amino acids 1 to 433) which is the part linked to stress-dependent stabilization. The DNA-binding region of NRF2 is not included in the construct to ensure that it has no biological activity. The expression of the luciferase-NRF2 fusion reporter is under control of a stress-inducible promoter, containing three ARE repeats. Therefore, the fusion protein is only expressed and stabilized under stress conditions when endogenous NRF2 is activated. The signal can be detected by standard luciferase assays (Figure 2(a)). When NRF2 activity decreases, the fusion protein is degraded via the KEAP1-proteasome pathway [28].

We generated HuH7 cells constitutively expressing the OKD48 reporter. Treatment of these cells with the oxidizing agent sodium arsenite (ASN) leads to robust induction of reporter activity (Figure 2(b)). To analyze NRF2 activity in *P. berghei*-infected cells, we infected the OKD48 expressing HuH7 cells with *P. berghei* sporozoites constitutively expressing mCherry (*Pb*mCherry). Because of the low infection rate, cells were sorted by FACS into an infected (90% +/−2% infected cells) and a noninfected population. At 6 hours post infection (hpi), a luciferase assay was performed, and the signal was normalized to the number of living cells in each sample. A statistically significant 2-fold increase in NRF2 activation was detected in infected cells compared to the noninfected control (Figure 2(b)).

To further analyze NRF2 activation, we generated *NRF2*$^{-/-}$ HuH7 cells using the CRISPR/Cas9 genetic manipulation system (Figure 2(c)). We chose a lentiviral approach for plasmid delivery to maximize efficiency. Two independent guideRNAs targeting exon 4 of the human *NRF2* gene were chosen. The plasmids containing the guideRNAs or Cas9 were transfected along with lentiviral envelope and packaging plasmids into HEK293T lentiviral producer cells. Lentiviral supernatant was harvested and used for transduction of HuH7 cells. Cells were transduced with two viruses, one containing a guideRNA construct and one the Cas9 cDNA. Four different *NRF2*$^{-/-}$ clones were obtained and confirmed by western blotting and subsequent genomic sequence analysis to be void of NRF2 protein (Figure 2(c)).

To confirm specificity of the OKD48 reporter used for analyzing NRF2 activation (Figure 2(b)), *NRF2*$^{-/-}$ HuH7 cells were transduced with the OKD48 reporter, treated with ASN, and NRF2 activation was analyzed by luciferase assay. As expected, no enhanced reporter activity was measured in *NRF2*-deficient HuH7 cells (Figure 2(d)).

2.2. p62 Leads to NRF2 Activation by Recruiting KEAP1 to the PVM. Since NRF2 can be activated in a p62-dependent manner and p62 was shown earlier to localize to the *Plasmodium* PVM during liver stage development [27], we further explored this mechanism of activation. We first confirmed p62 localization at the PVM in mouse primary hepatocytes by indirect immunofluorescence assay (IFA) using antibodies against p62 and "Upregulated in Infective Sporozoites 4" (UIS4), an exported parasite protein which localizes to the PVM (Figures 3(a) first panel and 3(b); Fig. S1C).

P62 can interact with KEAP1, thereby competing with NRF2. This leads to the stabilization of NRF2 and activation of NRF2 target genes [23]. Since phosphorylation of p62 at serine 349 (serine 351 in mice) increases the binding affinity for KEAP1, we next tested whether p62 at the PVM of *P. berghei* liver stage parasites is phosphorylated. We infected mouse primary hepatocytes with *Pb*mCherry parasites and performed IFAs using an antibody that specifically recognizes mouse p62 that is phosphorylated at S351. In this experiment, LC3 was used as a PVM marker since it is known to localize to the PVM of *Plasmodium* liver stage parasites [27, 29–31] (Fig. S1 A&B). Interestingly, p62 at the PVM is indeed phosphorylated at S351 (Figures 3(a), second panel and 3(b); Fig. S1C). This finding was also confirmed in HuH7 cells (Fig S1D). Also, costaining experiments revealed that the signal of p62 and phosphorylated p62 overlaps, confirming the specificity of the antibodies used for IFA (Figures 3(a), lowest panel and 3(b); Fig. S1C). Of note, in uninfected cells p62 phosphorylation at Ser349 was negligible confirming that it is indeed parasite infection and the formation of a PVM that causes activation of this pathway (Fig. S1D).

In a next step, KEAP1 localization was investigated by expressing a GFP-KEAP1 fusion protein in HuH7 cells. GFP-KEAP1 localization was analyzed by confocal microscopy and found to colocalize with p62 at the PVM of *Plasmodium* parasites in more than 80% of all parasites analyzed (Figures 3(c) first panel and 3(d)). Aiming to study whether KEAP1 recruitment to the PVM is dependent on p62, p62$^{-/-}$ HuH7 cells were generated using the CRISPR/Cas9 paired nickase approach. Two individual clones were confirmed to be deficient in p62 expression by western blot analysis (Figure 3(e)). In contrast to the pronounced GFP-KEAP1 localization to the PVM in WT cells, the p62$^{-/-}$ cells showed a rather even distribution throughout the cytoplasm (Figures 3(c) second panel and 3(d)). When transfecting p62$^{-/-}$ cells with mCherry-p62, KEAP1 association with the PVM was restored (Figures 3(c) third panel and 3(d)). Adding back p62 containing a mutation in the KEAP1-interacting region (KIR; threonine at position 350 mutated to alanine) did not restore PVM localization of KEAP1 (Figures 3(c) lowest panel and 3(d)). These findings confirm that KEAP1 is recruited to the PVM of *Plasmodium* parasites by the p62 KIR domain.

To address the question of whether KEAP1 recruitment to the PVM leads to NRF2 activation, we generated p62$^{-/-}$ cells with stably integrated OKD48 reporter. These cells were infected with *Pb*mCherry, sorted for infected (sorting rate 90% +/−2%) and noninfected cells, and reporter activity was measured at 6 hpi. Treatment with ASN was used as a positive control. While NRF2 activation could still be induced by ASN in the p62$^{-/-}$ cells, infection with *P. berghei*

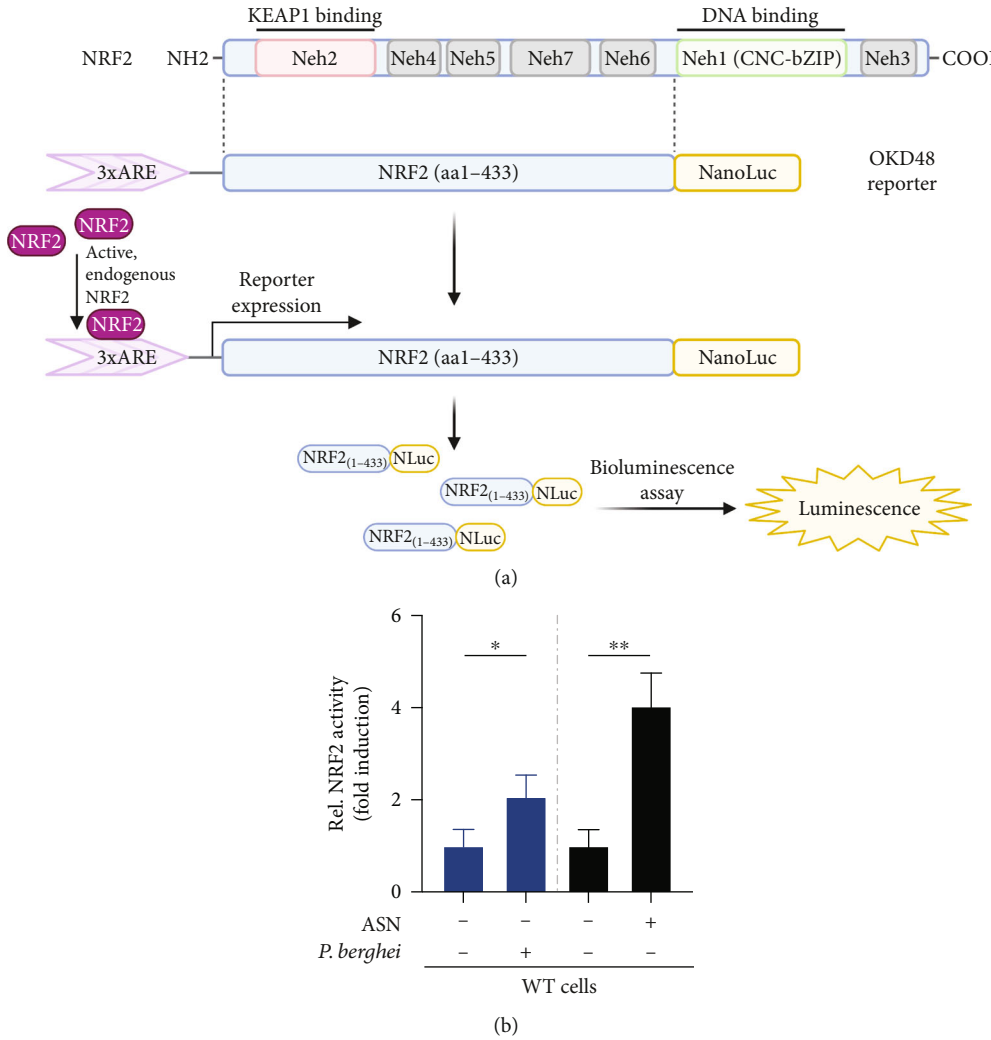

Figure 2: Continued.

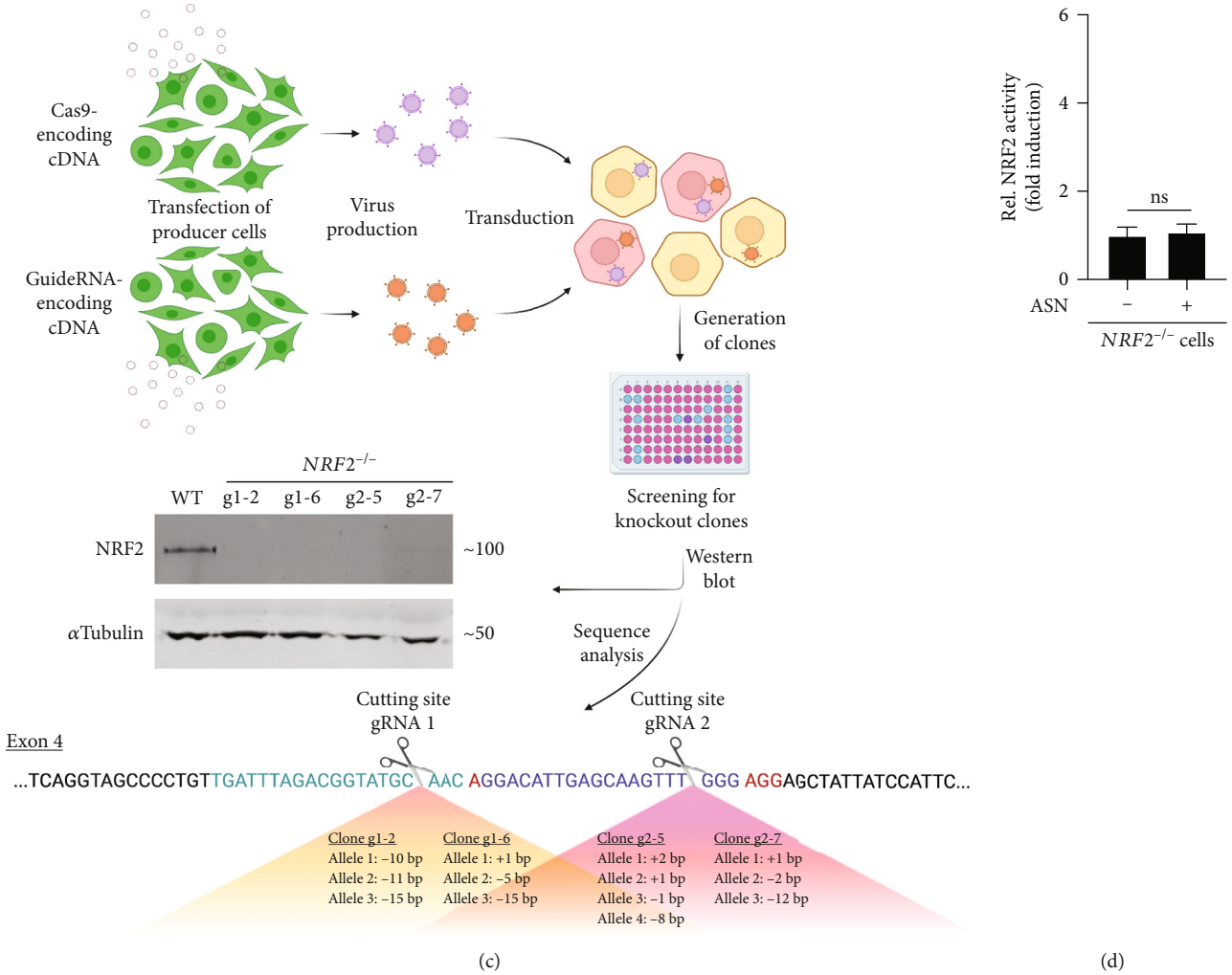

Figure 2: NRF2 is activated in *P. berghei* infected cells. (a) Schematic of the OKD48 reporter [28]. NRF2 is composed of 7 functional domains NRF2-ECH homology (Neh) domains 1-7. The Neh1 domain (green) contains the conserved CNC-bZIP region which functions in DNA binding. The Neh2 domain (red) is involved in KEAP1 binding and ubiquitination-dependent degradation. The reporter consists of amino acids 1-433 of human NRF2 (blue) fused to a NanoLuc luciferase (yellow). The fusion protein is controlled by an NRF2 inducible promoter containing 3 ARE sequences (violet). Endogenous NRF2 activation leads to the expression of the reporter and stabilization of the NRF2(1-433)-NLuc fusion protein which can be measured by standard bioluminescence assay. Schematic created with BioRender.com. (b) HuH7 cells stably transduced with the OKD48 NRF2-reporter construct [28] were infected with sporozoites constitutively expressing mCherry (*Pb*mCherry). 5 hours post infection (hpi) cells were sorted by FACS in an infected and a noninfected control population. As a positive control, cells were treated with 1 μM sodium arsenite (ASN) for 6 hours. 6 hpi, luciferase activity was measured, and the signal was normalized to the number of living cells in each sample. Sorted infected cells were compared to sorted noninfected cells, while ASN treated cells were compared to untreated cells. The graph shows the relative induction compared to the respective control. The experiment was carried out 3 times independently. Depicted are mean and SD. Significance was determined by *t* -test ($^{*}p \leq 0.05$ and $^{**}p \leq 0.01$). (c) Generation of *NRF2*$^{-/-}$ cells. HEK293T cells were transfected with either a Cas9-encoding plasmid or a plasmid encoding a single guideRNA and plasmids needed for lentiviral packaging and envelope. The viruses were harvested, and HuH7 cells were transduced with both the lentivirus containing the Cas9 and a virus containing one of the two guideRNAs. 2 different guideRNAs were used separately. Cells were then cloned out by limiting dilution and screened for knockout clones by western blot and sequencing. For the western blot, HuH7 WT cells and four different *NRF2* knockout clones were cultivated in growth medium containing 10 μM sodium arsenite and 10 μM MG-132 to accumulate NRF2 protein. After 8 hours, cells were lysed and western blot analysis was performed. Whole protein lysates were separated on a 10% acrylamide gel, blotted on a nitrocellulose membrane, and probed with an anti-NRF2 antibody. As a loading control α-tubulin was detected, the targeted sequence of *NRF2* exon 4 is depicted. In green and blue, the regions recognized by the two different guideRNAs are highlighted. Sequence analysis showed three to four alleles in all four clones obtained. Schematic created with BioRender.com. (d) HuH7 *NRF2*$^{-/-}$ cells (clone g2–5) stably transduced with the OKD48 NRF2-reporter construct [28] were treated with 1 μM sodium arsenite (ASN) for 6 hours. Subsequently, reporter activity was measured by luciferase assay and the signal was normalized to the number of living cells in each sample. The graph shows the relative induction compared to the nontreated control. Mean and SD of three independent experiments are depicted. The *P*-value was calculated using a Student's *t*-test (ns: $p > 0.05$).

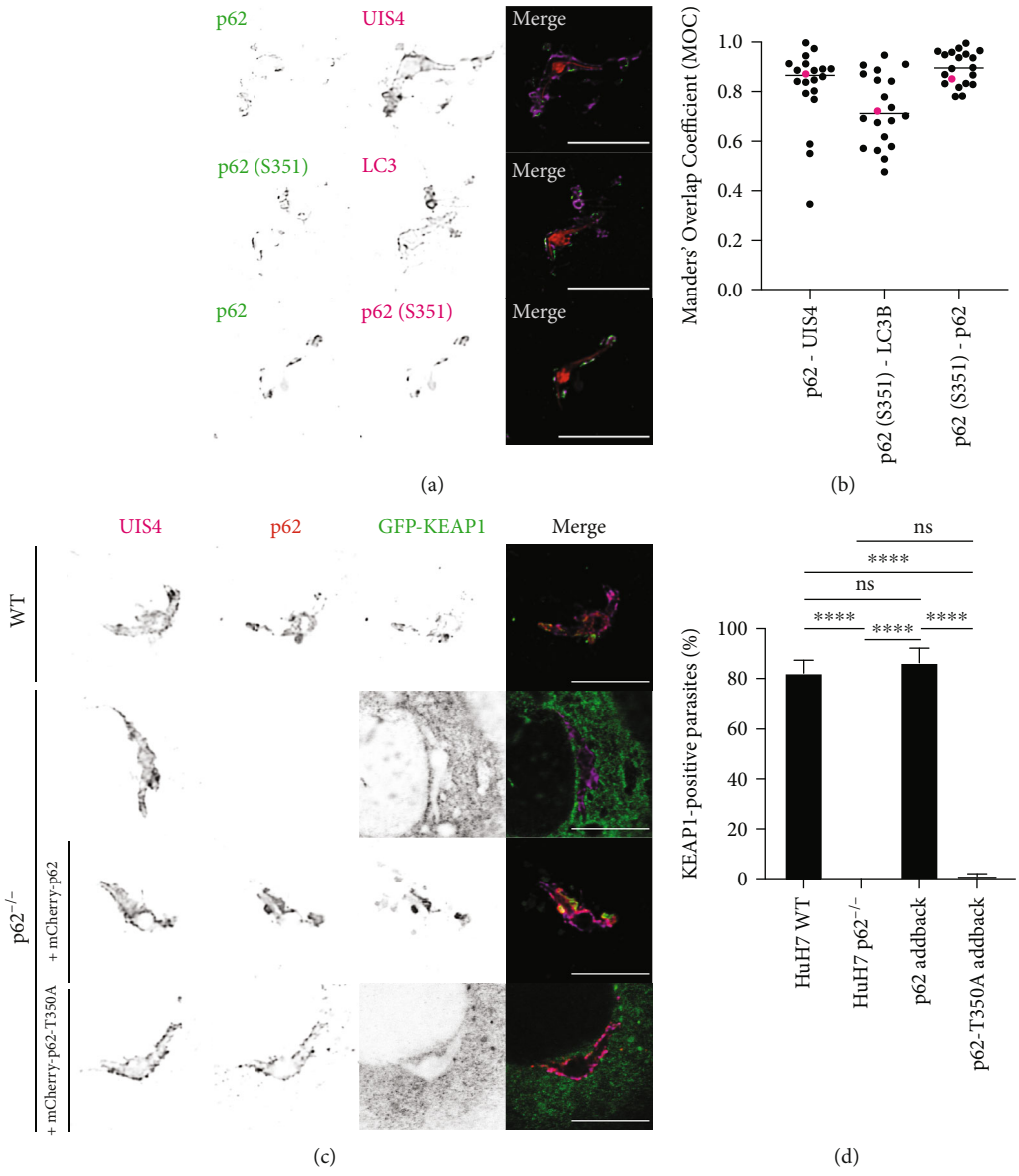

Figure 3: Continued.

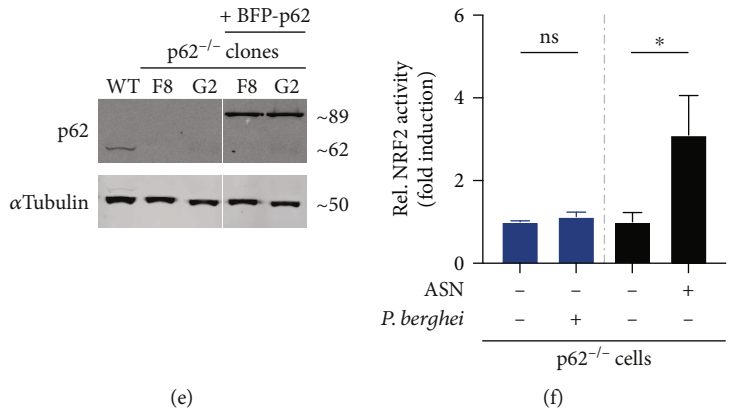

Figure 3: p62 activates NRF2 by recruiting KEAP1 to the PVM. (a) Primary mouse hepatocytes were infected with *Pb*mCherry parasites (red). 6 hpi, cells were fixed and stained with either anti-UIS4 (magenta; upper panel) or anti-LC3 antibodies (magenta; middle panel) to visualize the PVM. p62 was stained using an anti-p62 antibody or an antibody specifically recognizing p62 phosphorylated at serine 351. Images were taken at a confocal laser scanning microscope and deconvolved using Huygens Professional. Scale bar: 10 μm. Note that p62 localizes to the PVM and is phosphorylated at S351. (b) Quantification of (a). Graph shows Manders' Overlap Coefficient (MOC) for p62 and UIS4, phosphorylated p62 and LC3B, and phosphorylated p62 and p62. MOC was calculated using FIJI. $N = 20$ parasites per staining. Each dot represents one parasite with the pink dot representing the parasite shown in (a). (c) HuH7 WT (upper panel) and $p62^{-/-}$ (second panel) cells stably expressing GFP-KEAP1 (green) were infected with *P. berghei* wildtype sporozoites (*Pb*WT). 6 hpi, cells were fixed and stained with anti-UIS4 antibodies to visualize the PVM (magenta) and anti-p62 antibody (here in red). In addition, $p62^{-/-}$ cells were transiently transfected with either mCherry-p62 (third panel; red) or mCherry-p62-T350A (lowest panel; red). Images were taken by confocal microscopy and deconvolved with Huygens Professional. Note that p62 T350 is required for KEAP1 recruitment to the PVM. Scale bar: 10 μm. (d) Quantification of (c). The percentage of UIS4-positive parasites showing GFP-KEAP1 associations with the PVM was determined in all four conditions. The graph depicts mean and SD of three independent experiments. *P*-values were calculated using a one-way ANOVA test followed by Tukey's post hoc test (ns: $p > 0.05$ and $^{****}p \leq 0.0001$). $N = 100$ per experiment for WT and $p62^{-/-}$ cells. $N = 30$ per experiment for the addback conditions. (e) Confirmation of p62 knockout by western blot. HuH7 WT cells, two $p62^{-/-}$ clones, and the respective BFP-p62 addback cell lines were lysed, and western blot analysis was carried out. Whole protein lysates were run on a 12% SDS gel. p62 was detected using a mouse anti-p62 antibody. α-Tubulin was detected sequentially with a mouse anti-α-Tubulin antibody and used as a loading control. (f) HuH7 $p62^{-/-}$ cells (clone G2) stably transduced with the OKD48 NRF2-reporter construct [28] were infected with *Pb*mCherry sporozoites. 5 hours post infection (hpi) cells were sorted by FACS into an infected and a noninfected population. 6 hpi, luciferase activity was measured, and the signal was normalized to the number of living cells in each sample. As a positive control, cells treated with 1 μM sodium arsenite (ASN) for 6 hours were used. Sorted infected cells were compared to sorted noninfected cells, while ASN treated cells were compared to untreated cells. The graph shows the relative induction compared to the respective control. The experiment was carried out 3 times independently. Mean and SD are depicted. Significance was determined by *t*-test (ns: $p > 0.05$ and $^{*}p \leq 0.05$).

led to no increase in reporter activity (Figure 3(f)). This led to the conclusion that p62 is indeed involved in *Plasmodium*-dependent NRF2 activation.

2.3. NRF2 Activation Counteracts Oxidative Stress Generated by Plasmodium Infection. Since NRF2 is described to become primarily activated as a response to oxidative stress, we sought to investigate the redox status of *P. berghei*-infected cells. To this purpose, we deployed the genetically encoded GFP-based ratiometric reduction-oxidation sensitive probe roGFP2. roGFP2 is an engineered version of GFP containing two additional cysteine residues. The thiol groups of these cysteines form a disulfide bridge upon oxidation which leads to a shift in the excitation maximum of the fluorescent protein. This approach allows the monitoring of the redox status of cells by microscopy under physiological conditions. While roGFP2 in the reduced state shows an excitation maximum at 488 nm, this excitation peak is reduced and another excitation maximum appears at 405 nm in the oxidized state. The emission spectrum is not influenced. Thus, the ratiometric readout of the different excitation maxima allows the analysis of the redox status of the roGFP2-transfected cells [32].

We generated HuH7 WT and $NRF2^{-/-}$ cells stably expressing roGFP2 in their cytoplasm. To ensure the accurate functioning of the reporter, WT roGFP2 cells were treated with different concentrations of hydrogen peroxide (H_2O_2). Cells were imaged by confocal microscopy, and the ratio of signal intensities at both excitation peaks was calculated. The oxidation state of the cells rose with increasing H_2O_2 concentration to a maximum of around 3-fold compared to nontreated cells (Figure 4(a)), confirming the functionality of the reporter. Very similar results were achieved when using ASN instead of H_2O_2 to induce oxidative stress (Fig. S2). Additionally, some cells were followed by confocal live-cell microscopy while changing oxidation state by first adding H_2O_2 and subsequently reducing them using normal growth medium and increasing concentrations of dithiothreitol (DTT) (Figure 4(b)). The response to the treatments was rapid and very consistent between all the cells analyzed.

Having confirmed the functionality of roGFP2 as a redox detector, WT and $NRF2^{-/-}$ cells expressing roGFP2 were used for infection with *P. berghei* sporozoites. Infected and noninfected cells were imaged 6 hpi by confocal microscopy, and the ratio of signal intensities at both excitation peaks was

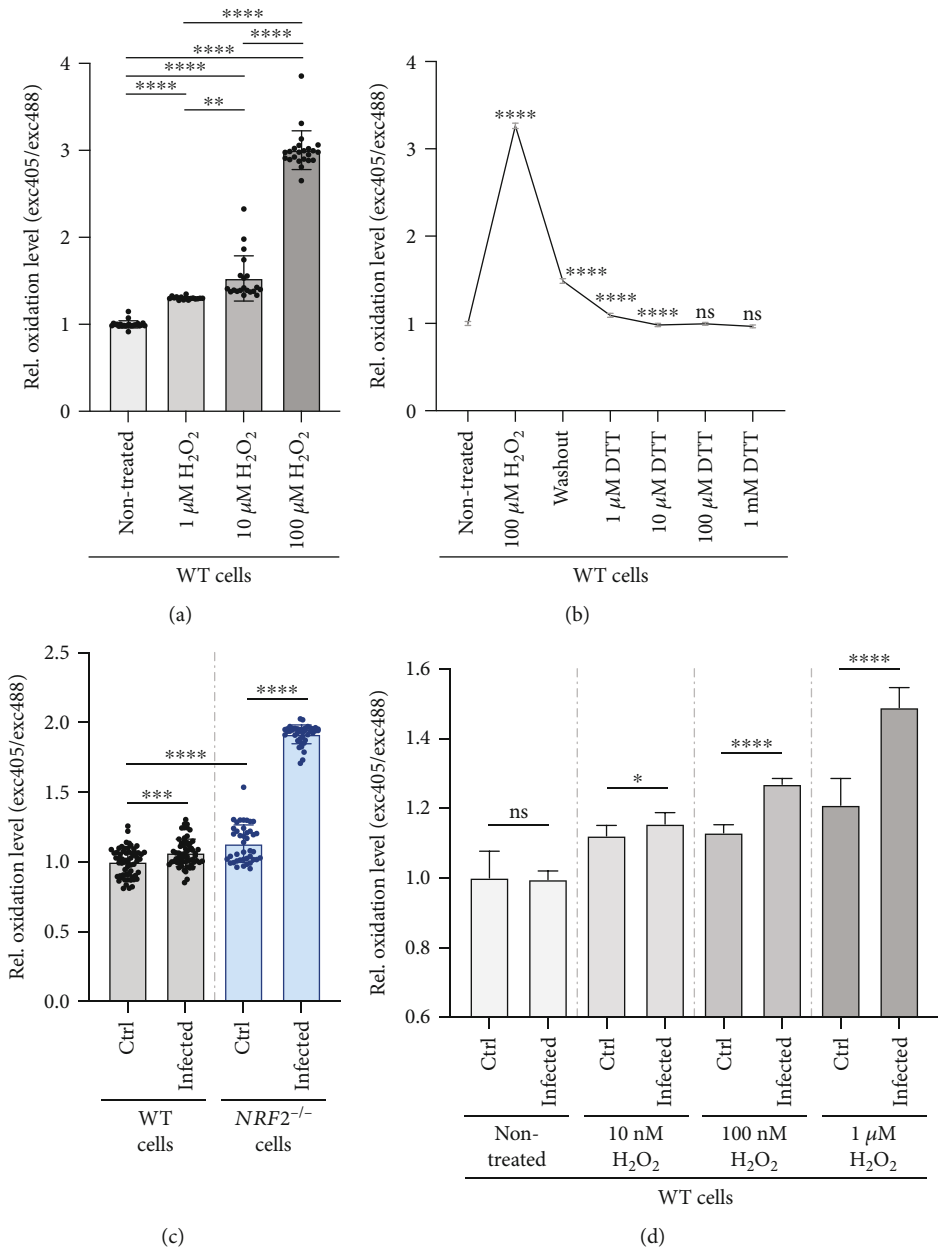

Figure 4: NRF2 activation counteracts ROS generation in *P. berghei* infected cells. (a) HuH7 WT cells stably expressing roGFP2 in the cytoplasm were treated with different concentrations of H_2O_2 to induce oxidative stress. Single cells were imaged once with excitation 405 nm and once with excitation 488 nm with the same detection range of 500 nm to 550 nm. Signal intensities for both excitation wavelengths were measured using FIJI. The graph depicts the ratio of both signal intensities which each dot representing one single cell. $N = 20$ per condition. Graph shows mean and SD. *P*-values were calculated using a one-way ANOVA test followed by Tukey's post hoc test ($^{**}p \leq 0.01$ and $^{****}p \leq 0.0001$). (b) Nontreated HuH7 roGFP cells were imaged, then treated with first 100 μM H_2O_2 and sequentially reduced again with growth medium containing DTT at different concentrations. The same cells were followed over the different treatments. $N = 10$. The significance to the respective previous treatment was calculated using a Student's *t*-test (ns: $p > 0.05$ and $^{****}p \leq 0.0001$). (c) HuH7 WT and *NRF2*$^{-/-}$ cells stably expressing roGFP2 in their cytoplasm were infected with *Pb*mCherry. 6 hpi, infected and noninfected cells were imaged using confocal microscopy. Each cell was imaged once with excitation 405 nm and once with excitation 488 nm with the same detection range of 500 nm to 550 nm. Signal intensities for both excitation wavelengths were measured using FIJI. The graph shows the ratio exc405/exc488 with each dot representing one single cell. $N = 60$ in wildtype cells and $N = 40$ in *NRF2*$^{-/-}$ cells. *P*-values were determined using a Student's *t*-test ($^{***}p \leq 0.001$ and $^{****}p \leq 0.0001$). (d) HuH7 WT cells stably expressing roGFP2 were infected with *Pb*mCherry. 6 hpi, infected and noninfected cells that were either left untreated or treated with different concentrations of H_2O_2 were imaged as described above. The graph depicts the ratio of signal intensity with excitation 405 nm divided by signal intensity at excitation 488 nm. Each dot represents one single cell. The experiment was carried out twice with $N = 10$ per condition. One representative experiment is shown. Significance was determined by Student's *t*-test (ns: $p > 0.05$; $^{*}p \leq 0.05$; and $^{****}p \leq 0.0001$). Note that different scales were used in (a),(c), and (d) for optimal display of small differences.

calculated. In WT cells the oxidation level was only slightly higher in infected compared to noninfected cells, suggesting that infection does not greatly affect the oxidation level of the host cell. However, when *NRF2*$^{-/-}$ cells were infected, a pronounced increase in oxidation levels was observed (Figure 4(c)). This led to the hypothesis that WT cells counteract infection-induced oxidative stress in an NRF2-dependent manner. To test this hypothesis, we decided to treat WT cells in addition to infection by adding oxidizing agents. We reasoned that chemical oxidation should have a stronger effect in infected cells because they experience an additional oxidation by infection, which cannot be fully compensated by NRF2 activation. Indeed, treatment with H_2O_2 resulted in significant higher oxidation levels in infected cells compared to noninfected cells even at low concentrations. Increasing H_2O_2 concentrations strongly enhanced this effect in infected cells (Figure 4(d)) suggesting that infection already pushes the NRF2 compensation of oxidation level to its limits. Indirectly, this indicates that infection leads indeed to the formation of ROS which can be neutralized by the host cell to a certain extent in an NRF2-dependent manner. This also means that in *P. berghei*-infected cells, ROS are not a prime activator of NRF2, and the p62-dependent recruitment of KEAP1 is the main pathway for NRF2 activation.

2.4. NRF2 Activation Enhances Parasite Survival. Since NRF2 activation leads to the expression of genes involved in cell protection and survival, we hypothesized that this might be beneficial for parasite survival. *In vivo* analysis of parasite load in the liver of infected *Nrf2*$^{-/-}$ mice showed a slight tendency towards a lower parasite load, but this was not significant compared to WT mice (Fig. S3A). Since *Nrf2* knockout animals in general showed no obvious phenotype or developmental impairment, we reasoned that they might have compensated the loss of such a central transcription factor and therefore set up an *in vitro* assay to investigate parasite survival under more controlled conditions. Analysis of the development of mCherry-expressing parasites by automated high throughput live cell imaging allowed investigation of parasite survival rate between 6 hpi and 48 hpi and assessment of parasite size. While we were not able to detect a significant phenotype in parasites developing in primary hepatocytes isolated from *Nrf2*$^{-/-}$ mice (Fig. S3 B&C), we found that parasite survival in HuH7 *NRF2*$^{-/-}$ cells was reduced to less than 40% compared to parasites infecting WT cells (Figure 5(a)). Interestingly, the size of the parasites at 48 hpi was not affected by the knockout (Figure 5(b)). We next aimed to perform addback experiments to confirm that the impaired survival rate in *NRF2*$^{-/-}$ cells was specific. However, since NRF2 levels in the cell are tightly regulated, exogenous expression led to cell death, and thus this addback experiment could not be performed.

We therefore decided to repeat the survival experiment with the upstream interaction partner of NRF2, p62. Importantly, knocking out p62 in HuH7 cells also led to a reduced parasite survival to a similar extent as in *NRF2*$^{-/-}$ cells. This phenotype could be compensated when adding back a BFP-p62 construct (Figure 5(c)). Parasite size in p62$^{-/-}$ cells was not significantly altered. However, in host cells expressing add back p62, parasites grew significantly bigger than in the p62$^{-/-}$ cells (Figure 5(d)). This suggests that p62 has other functions in supporting parasite growth.

In summary, these data obtained in *NRF2*$^{-/-}$ and p62$^{-/-}$ cells indicate that NRF2 activation through the p62-dependent pathway plays a crucial role in parasite survival.

3. Discussion

Host cell survival is critical for the successful development and reproduction of intracellular pathogens. Many intracellular pathogens, including viruses, bacteria, and parasites, are known to interfere with host apoptosis either directly or through hijacking of signal transduction pathways [33, 34]. While it was previously shown that *Plasmodium* parasites interfere with host cell apoptosis by rendering the infected hepatocyte resistant to apoptosis [7], the exact mechanism behind this phenomenon is not known yet. In this paper we provide evidence for the prosurvival transcription factor NRF2 to be involved in survival of *Plasmodium* parasites during liver stage development.

We have previously shown that the well-known selective autophagy receptor p62 interacts with LC3 at the PVM of *Plasmodium* liver stage parasites. However, in contrast to the expectations, p62 is dispensable for autophagic targeting of the parasite [27]. This suggested that p62 might have a function different than autophagy. p62 was described to participate in many different cellular processes, including NRF2 signaling [35]. Activation of the transcription factor leads to transcriptional induction of genes mainly involved in oxidative stress response, xenobiotic metabolism, and cell survival. Given the diverse cellular processes that NRF2 controls, its regulation is very complex and multifactorial. In this paper, we analyzed NRF2 activation in *Plasmodium*-infected cells by p62-dependent NRF2 stabilization. Indeed, we found the transcription factor to be activated upon infection in a p62-dependent manner by sequestration of KEAP1 to the PVM (Figure 6). However, NRF2 activity is not only controlled by regulating protein stability but also at the transcriptional and post-transcriptional level (reviewed in [36]). Several other cytoplasmic proteins that interfere with the KEAP1-NRF2 interaction and therefore influence NRF2 activity have also been identified. Among these are partner and localizer of BRCA2 (PALB2) [37], phosphoglycerate mutase 5 (PGAM5) [38], dipeptidyl-peptidase 3 (DPP3) [39], and Wilms tumor gene on X chromosome (WTX) [40]. However, since in infected p62-deficient HuH7 cells NRF2 activity was negligible, p62 appears to be the main pathway for NRF2 activation in infected cells.

ROS play an important role in intracellular immune response to pathogens such as bacteria or parasites [41, 42]. It was shown previously that ROS generated by fatty acid beta-oxidation impact *Plasmodium* development [43]. Here we found that NRF2 is required to balance oxidative stress levels in hepatocytes infected with *P. berghei* parasites, since in infected *NRF2*$^{-/-}$ cells oxidative stress levels were significantly higher compared to infected WT cells. Furthermore, infected cells are observed to be more sensitive to

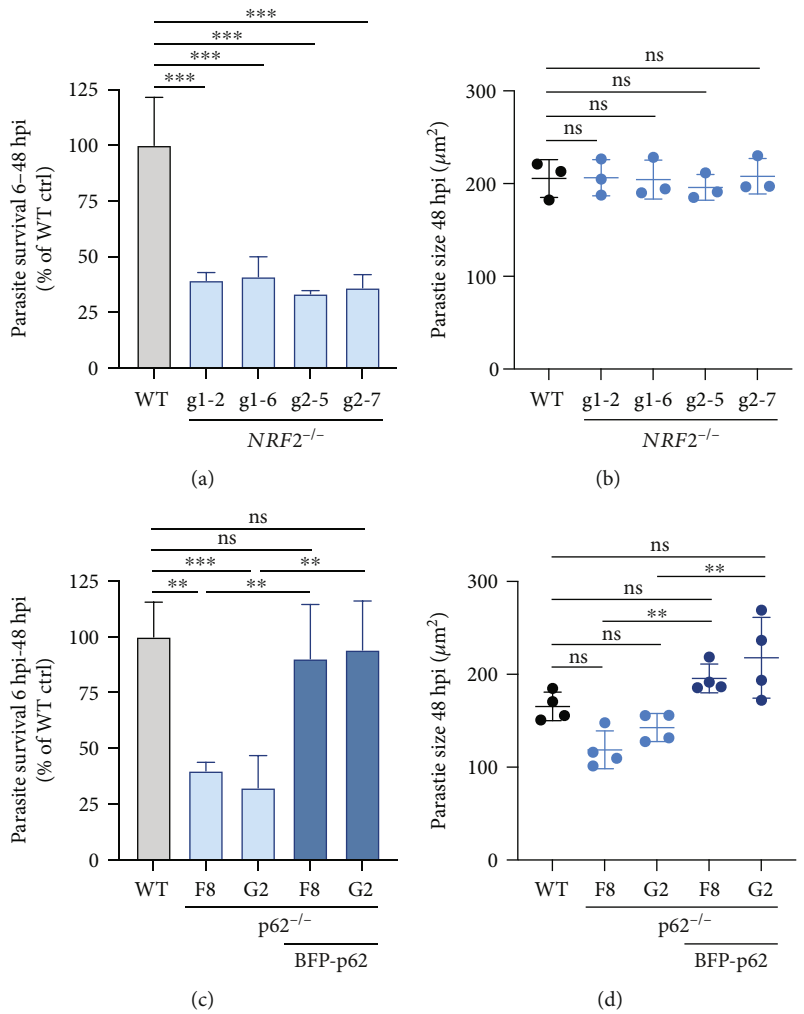

Figure 5: Parasite survival is reduced in *NRF2*-deficient cells. (a) HuH7 WT and 4 different *NRF2*$^{-/-}$ clones were infected with *Pb*mCherry. At 6 and 48 hpi, parasite numbers were evaluated using automated high throughput live cell imaging and analysis (InCell Analyzer 2000). The graph shows relative parasite survival from 6 to 48 hpi compared to the WT control. Mean and SD of three independent experiments are depicted. $N > 1400$ parasites per cell line and experiment. A one-way ANOVA test coupled to a Tukey's post hoc test was used to determine *P*-values ($^{***}p \leq 0.001$). (b) Parasite size at 48 hpi of experiment described in (a). The graph shows the medians in parasite size of >200 parasites per cell line and experiment. The experiment was performed 3 times. Mean and SD are depicted. $N > 200$ parasites per cell line and experiment. *P*-values were calculated using a one-way ANOVA test followed by Tukey's post hoc test (ns: $p > 0.05$). (c) HuH7 WT and 2 different p62$^{-/-}$ clones with the corresponding addback cell lines were infected with *P. berghei* parasites expressing GFP (*Pb*GFP). Parasite survival in the different cell lines was determined as in (a). The graph shows the relative survival compared to the WT control. Mean and SD of three independent experiments are shown. $N > 400$ parasites per cell line and experiment. *P*-values were calculated using a one-way ANOVA test coupled to Tukey's post hoc test (ns: $p > 0.05$; $^{**}p \leq 0.01$; and $^{***}p \leq 0.001$). (d) Parasite size at 48 hpi of the experiment described in (c). The graph shows the medians in parasite size of 4 experiments. $N > 100$ parasites per cell line and experiment. Mean and SD are depicted. *P*-values were determined using a one-way ANOVA test followed by Tukey's post hoc test (ns: $p > 0.05$; $^{**}p \leq 0.01$; and $^{***}p \leq 0.001$).

oxidative agents than noninfected cells, suggesting that NRF2-dependent antioxidant response programs are already at their limits upon infection.

Interestingly, it has recently been described that ROS-dependent host cell death plays a role in eliminating *Plasmodium* parasites during liver stage through a process called ferroptosis [44]. Ferroptosis is characterized by accumulation of lipid peroxidation products and ROS derived from iron metabolism [45]. The tumor suppressor p53 has been identified as a positive regulator of ferroptosis [46]. In *Plasmodium*-infected cells, p53 levels were found to be substantially decreased [47] protecting infected cells from ferroptosis and favoring parasite survival. Furthermore, the negative regulator of ferroptosis, SLC7a11 was shown to be important for liver stage development [44]. Interestingly, expression of SLC7a11 is regulated by NRF2 [48] confirming that the presence of the parasite regulates the oxidative state of its host cell. Since NRF2 functions in inhibiting ferroptosis mainly by controlling intracellular oxidation homeostasis [49–51], it will be interesting to investigate whether there is a

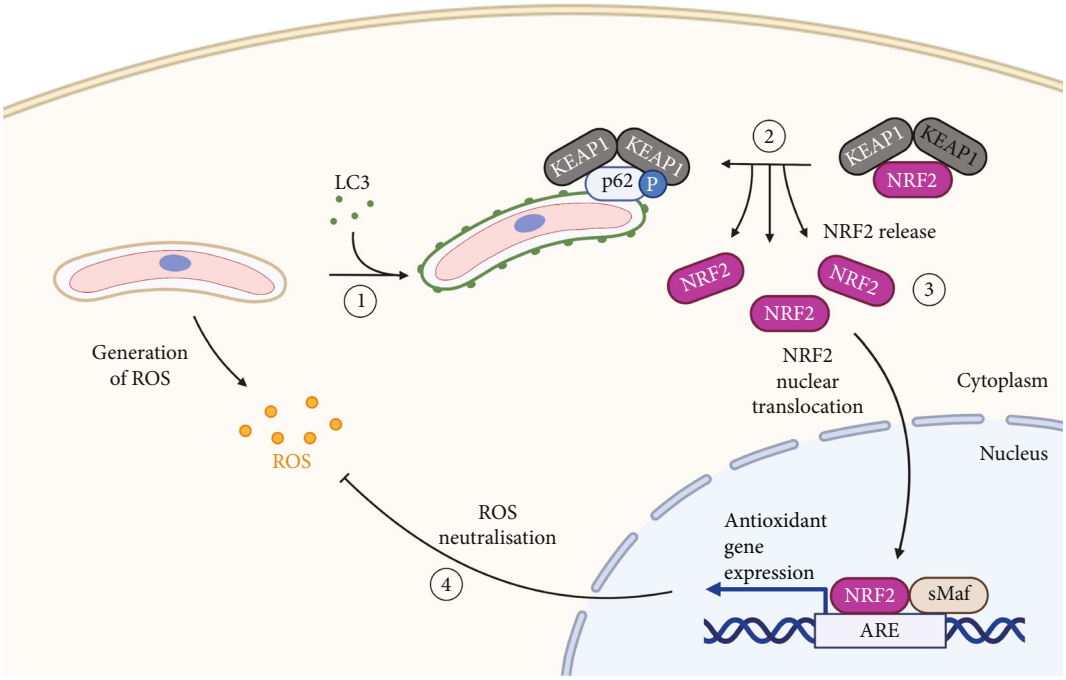

Figure 6: Schematic representation of NRF2 activation in *P. berghei* infected hepatocytes. (1) Immediately after infection, the PVM of *P. berghei* parasites is labelled with host cell LC3 which is known to recruit p62 to the PVM [27]. (2) p62 at the PVM is phosphorylated at S349 (S351 of mouse p62) and recruits KEAP1. (3) KEAP1 interaction with p62 leads to the release and therefore to the activation of NRF2. (4) NRF2 activation enhances parasite survival by controlling oxidation levels that are elevated by infection with *Plasmodium*. Schematic created with BioRender.com.

link between the activation of NRF2, ferroptosis, and parasite survival.

In *Plasmodium* blood stage infection, high oxidative stress in the brain of mice suffering from experimental cerebral malaria was shown to induce NRF2 activation using transgenic mice expressing the OKD48 NRF2 reporter [52]. One of the best studied NRF2 target genes is heme oxygenase-1 (Hmox1) which promotes the degradation of free heme and reduces ROS. Interestingly, Hmox1 was shown to be upregulated and even critical for the promotion of *Plasmodium* liver stage infection *in vivo* [53]. A recent study analyzing the transcriptome of single infected hepatocytes confirmed upregulation of Hmox1 among several other Nrf2 targets in *Plasmodium berghei*-infected hepatocytes. Among these are proteins involved in glutathione and iron metabolism such as glutathione S-transferases (Gstm1 and Gstm3) and Ftl1, Fth, and Slc40a1, respectively. In addition, p62 expression that is also controlled by Nrf2 was found to be upregulated in infected host cells [13]. Another recent transcriptome analysis on cells infected with *Plasmodium vivax*, a human infecting *Plasmodium* species, found enrichment of transcripts governed by NRF2 upon infection of primary human hepatocytes. Upregulation of genes controlled by NRF2 was observed in all infected cells, suggesting a broad importance of the transcription factor for parasite persistence and survival [14]. These transcriptome studies strongly support our findings that NRF2 is constitutively activated during *Plasmodium* infection of hepatocytes.

Importantly, NRF2 activation is not restricted to *Plasmodium* infection of hepatocytes but seems to be a common response to infection of host cells by a wide variety of intracellular pathogens. Most intensively studied are viral infections. One of the best described examples is Marburgvirus (MARV), where a viral protein is capable of binding directly to KEAP1 and therefore activates NRF2. This is coupled to a higher replication rate of the virus, suggesting that MARV developed a mechanism to employ the host cell's antioxidant response as a survival strategy (reviewed in [54]).

Infections with protist parasites were also reported to trigger NRF2 responses. A recent study reported that infection with *Toxoplasma gondii*, another apicomplexan parasite closely related to *Plasmodium*, leads to NRF2 activation in the host cell. The authors demonstrated that activation occurs in a p62-dependent manner. Activation of NRF2 was shown to be crucial for parasite growth [55]. Moreover, infection with *Leishmania* was also shown to activate the NRF2 pathway as *NRF2*-deficient cells were shown to exhibit decreased parasite load [56].

The fact that infection of *Nrf2*$^{-/-}$ mice with *Plasmodium* sporozoites did not lead to a significant reduction in parasite load (Fig. S3A) could be due to genetic compensation. Genetic compensation as a response to gene knockout is a widespread phenomenon in *in vivo* studies. Transcriptional adaptation by upregulation of related genes following a gene knockout was observed in many studies involving small animal models (reviewed in [57]). In the case of Nrf2, this might be conceivable since Nrf2 is involved in different cellular responses and cells exhibit complex signaling networks with partly overlapping functions. The fact the deletion of such a central transcription factor as Nrf2 did not result in

a substantial phenotype of the knockout animals strongly points in this direction [9, 58]. However, while mice in many respects mirror human biology well, we cannot exclude that the discrepancy between the experiments performed in human HuH7 cells, and the experiments done in mice or primary mouse hepatocytes reflects a different function of NRF2 in both species upon *Plasmodium* infection.

Together, we show that NRF2 activation is driven by p62 recruiting KEAP1 to the PVM of *Plasmodium berghei* parasites and that this activation is an important factor for optimal parasite development. This is another example of how parasites subvert host cell signaling pathways to ensure their own survival.

4. Experimental Procedures

4.1. Experimental Animals at University of Bern. Mice used in the experiments were between 6 and 12 weeks of age and were bred in the central animal facility of the University of Bern. Animal experiments were performed in strict accordance to the guidelines of the Swiss Tierschutzgesetz (TSchG; Animal Rights Laws) and approved by the ethical committee of the University of Bern (license number: BE86/19).

4.2. Common Parasite Strains. All parasite strains used have a *P. berghei* ANKA background. *Pb*mCherry, *Pb*GFP, and *Pb*mCherry$_{hsp70}$-Luc$_{eef1\alpha}$ parasites are phenotypically wild type (*Pb*WT) like. *Pb*mCherry express cytosolic mCherry under the control of the *P. berghei* hsp70 regulatory sequences [59]. *Pb*GFP parasites express cytosolic GFP under the promoter of the eukaryotic elongation factor 1-alpha (eef1α) [60]. *Pb*mCherry$_{hsp70}$-Luc$_{eef1\alpha}$ parasites (alternative name *Pb*1868cl1) express cytosolic mCherry under the control of the *P. berghei* hsp70 regulatory sequences and a firefly luciferase under the control of the eef1α promoter [29].

4.3. Culture, Treatment, and In Vitro Infection of HuH7 Cells and Primary Hepatocytes. HuH7 cells (Japanese Collection of Research Bioresources Cell Bank JCRB0403) were cultured in Minimum Essential Medium with Earle's salts (MEM EBS; BioConcept, 1-31F01-I), supplemented with 10% FCS (GE Healthcare), 100 U penicillin, 100 μg/ml streptomycin, and 2 mM L-glutamine (all from Bioconcept). Cells were cultured at 37°C and 5% CO_2 and split using Accutase (Innovative Cell Technologies). For oxidative stress related treatments, HuH7 cells were incubated in media containing the indicated concentration of sodium arsenite (Fisher Scientific 12897692) for 6 hours, H_2O_2 (Merck 107209) or DTT (Sigma-Aldrich D0632) at the indicated concentrations for 2–5 minutes. For western blotting of NRF2, cells were treated with 10 μM sodium arsenite and 10 μM MG-132 (Sigma-Aldrich M7449) for 8 hours.

Primary murine hepatocytes were isolated as described elsewhere [29] and cultured in William's E medium (Bioconcept 1-48F02-I) supplemented with 10% FCS (GE Healthcare), 100 U penicillin, 100 μg/ml streptomycin, and 2 mM L-glutamine (all from Bioconcept)at 37°C and 5% CO2.

For infection of cells, salivary glands of infected *Anopheles stephensi* mosquitoes were isolated and disrupted to release sporozoites. Sporozoites were incubated with cells in the respective medium.

4.4. Plasmids. The plasmids encoding mCherry-p62 and mCherry-p62-T350A were a generous gift of Dr. Conrad C. Weihl (Washington University in St. Louis, USA; [61]). The pEBFP2-LC3 plasmid was generated as described previously [62]. The plasmid used for expression of hrGFP-KEAP1 was a gift from Qing Zhong (Addgene #28025; [63]). To generate HuH7 cells constitutively expressing GFP-KEAP1, the GFP-KEAP1 open reading frame was amplified using primers 5′-CTCGAGCCGCTAGCACCAT GGTGAG-3′ and 5′-AGATATCTCAACAGGTACAGT TCTGCTGG-3′ and subcloned via NheI and EcoRV restriction sites into the pLX307 lentiviral vector. The plasmid used for stable BFP-p62 addback was generated by exchanging the mCherry from the mCherry-p62 plasmid described above with an eBFP2. Then, eBFP2-p62 subcloned into the pLX307 vector by restriction digest with NheI and SmaI. The plasmid for generation of HuH7 cells stably expressing roGFP in their cytoplasm was generated by PCR amplification of roGFP from the cyto-roGFP plasmid (a gift from Paul Schumacker; Addgene #49435; [64]) using primers 5′ -CTCGAGATGGTGAGCAAGGGCGAG-3′ and 5′-GGAT CCTTACTTGTACAGCTCGTCCATG-3′ and subsequent cloning into the lentiviral vector pLVX by XhoI and BamHI restriction digest. The OKD48 reporter plasmid (p(3xARE) TKbasal-hNrf2 (1-433)-GL4-F) was a kind gift of Prof. Takao Iwawaki (Kanazawa Medical University, Japan [28]). For stable transfection of HuH7 cells with this reporter, it was PCR amplified using primers 5′-ATCGATACTAG TGGAAATGACATTGC-3′ and 5′-GTCGACTTACTTGT CATCGTCATCCT-3' and subcloned via ClaI and SalI restriction sites into pRRLSIN.cPPT.PGK-GFP.WPRE. In a next step, the GL4 luciferase was exchanged by a NanoLuc luciferase by XhoI and SalI restriction digest. Virus production and transduction of cells were done as described previously [65]. The VSV-G envelope expressing plasmid pMD2. G (Addgene plasmid #12259), the 2nd generation packaging plasmid psPAX2 (Addgene plasmid #12260) and lentiviral expression plasmid pRRLSIN.cPPT.PGK-GFP.WPRE (Addgene plasmid #12252) were generous gifts from Didier Trono.

4.5. Transfection of Cells. HuH7 cells were harvested by Accutase treatment and 1×10^6 cells were pelleted by centrifugation at 700 g for 3 min at room temperature. Cells were resuspended in Nucleofector V solution (Lonza, VVCA-1003) and transfected with 1 μg of plasmid DNA using program T-028 of the Nucleofector 2b transfection device according to the manufacturer's instructions.

4.6. Generation of Knockout Cell Lines. The CRISPR/Cas9 paired nickase approach described by [66] was used to knock out the p62 gene. CRISPR guide RNA pairs (gRNAs) were designed to target exon 3. Cloning of the guideRNA

sequences into the plasmid pX335-U6-Chimeric_BB- CBh-hSpCas9n(D10A), (a gift from Feng Zhang; Addgene #42335; [67]), was performed following the protocol of the Zhang laboratory [68]. GuideRNAs 5′-TTGTAGCGGGT TCCTACCAC-3′ and 5′-AGGGAAAGGGCTTGCACCG-3′ were used. HuH7 cells were transfected with the pair of pX335 plasmids, each encoding for one guideRNA and Cas9 nickase, and the plasmid pcDNA3.1-Puro-mCherry-C1 (a gift from Erich Nigg, Basel, Switzerland). Transfection was performed following the protocol described above. Transfected cells were selected with 1 μg/ml puromycin for 3 days after transfection. Thereafter, selected cells were cultivated for 10 days before being plated in 96-well plates. Single colonies were expanded and screened for the absence of the respective protein by western blotting.

For the generation of *NRF2*$^{-/-}$ cells, the CRISPR/Cas9 GeCKO v2 lentiviral system was used, as described by the Zhang laboratory [69]. This two-vector system consists of a plasmid encoding for the human optimized Streptococcus pyogenes Cas9 (hSpCas9) enzyme (pLentiCas9-Blast; a gift from Feng Zhang; Addgene #52962; [69]) and a plasmid encoding for the single-guideRNA (pLentiGuide-Puro; a gift from Feng Zhang; Addgene #52963; [69]). GuideRNAs were chosen to target exon 4 of the human *NRF2* gene. Clones g1-2 and g1-6 were generated with the gRNA 5′-TGATTTAGA CGGTATGCAAC-3′ while clones g2-5 and g2-7 were generated using the gRNA 5′-GGACATTGAGCAAGTT TGGG-3′. gRNAs were cloned into the plasmid according to the protocol of the Zhang laboratory [69]. Lentiviruses were generated as described previously [65]. HuH7 cells were transduced with both viruses (guideRNA- and Cas9-encoding) and selected from 2 days after transduction with 1 μg/ml puromycin and 4 μg/ml blasticidin for 3 days. Single cell knockout clones were obtained and confirmed by western blotting and sequencing of the genomic locus using primers 5′-GTAGTGGTGCCTTAGAGCTTACTCATCC-3′ and 5′- CTAGCATGGGCAGTACTCATGACTAAG-3′ [70] (Figure 2(c)).

4.7. Protein Lysates and Western Blotting. Cells were seeded into 6-well plates to reach confluency the next day. Twenty-four hours later, after the appropriate treatment, cells were rinsed with PBS and lysed directly in the well with 200 μl Laemmli sample buffer (2% glycerol, 25 mM Tris HCl pH 6.8, 0.8% SDS, 0.004% bromophenolblue, 2% 2-mercaptoethanol) heated to 95°C. Next, the lysate was transferred to an Eppendorf tube and treated with universal nuclease (Thermo Fisher Scientific, 88701) for 5 min at room temperature. Proteins were denatured at 95°C for 5 min. To detect NRF2, the proteins were separated on 10% SDS PAGE. For detection of p62, 12% SDS PAGE was used. PageRuler Prestained NIR Protein Ladder (Thermo Fisher Scientific, 26635) was used as a molecular weight marker. The transfer to nitrocellulose membranes was performed in a tank blot device (Hoefer). Five percent fat free milk in TBST (Tris-buffered saline with Tween20; 10 mM Tris, 150 mM NaCl, 0.05% Tween 20) was used for blocking the membranes and antibody incubation. Antibodies used were rabbit mAB anti-NRF2 (Cell Signaling Technology, 12721, 1 : 1000), mouse monoclonal anti-p62 (MBL international, M162-3, 1 : 1,000), and mouse anti-α-tubulin (Sigma-Aldrich, T6199, 1 : 2000). For secondary antibody incubation, anti-rabbit or anti-mouse IgG 800 CW IRDye and anti-mouse IgG 680 LT IRDye (Li-Cor Biosciences, all 1 : 10,000) were diluted in 5% milk in TBST. A Li-Cor Odyssey Imaging system (Li-Cor Biosciences) was used for detection.

4.8. Indirect Immunofluorescence Analysis. After the indicated time periods, cells grown on glass cover slips were fixed with 4% paraformaldehyde in PBS for 8 min. Subsequently, they were permeabilized in 0.05% Triton X-100 (Fluka Chemie, T8787) in PBS for 5 min. Mouse primary hepatocytes were permeabilized using 100 μg/ml Digitonin (Sigma-Aldrich, D141) for 10 min. Unspecific binding sites were blocked by incubation in 10% FCS/PBS for 10 min. Cells were then incubated with primary antibody diluted in 10% FCS/PBS for 1 hour. The primary antibodies used were rabbit anti-UIS4 antiserum (1 : 5000), mouse monoclonal anti-p62 antibody (MBL, M162-3; 1 : 1000), rabbit polyclonal anti-phospho-Ser351-p62 (provided by Prof. Yoshinobu Ichimura, Juntendo University, Japan; 1 : 500), rabbit monoclonal anti-phospho-Ser349-p62 (Abcam, ab211324; 1 : 500), and mouse monoclonal anti-LC3 antibody (MBL M152-3; 1 : 1000). After washing with PBS, cells were incubated with fluorescently labelled secondary antibodies 1 : 1000 in 10% FCS/PBS for 1 hour. Secondary antibodies were anti-rabbit Alexa488 (Invitrogen, A-11008), anti-rabbit Cy5 (Dianova), anti-mouse Alexa488 (Invitrogen, A-11001), anti-mouse Cy5 (Dianova), and anti-mouse Alexa594 (Invitrogen, A-11032). All steps were carried out at room temperature. Labelled cells were mounted on microscope slides with ProLong® Gold Antifade mounting medium (Thermo Fisher Scientific, P36930).

4.9. Microscopy and Quantifications. Live cell imaging of roGFP-expressing cells was performed using an inverted Leica TCS SP8 using a HC PL APO CS2 63×/1.4 NA immersion oil objective. The pinhole was set to 2 AU to allow more light to pass. Excitation wavelengths were 405 nm and 488 nm, the emission detection range was set to 500–550 nm. During imaging, cells were kept in 5% CO_2 at 37°C. FIJI was used to measure signal intensities and to calculate the ratio.

Confocal images of fixed primary hepatocytes and HuH7 cells were acquired with an inverted Leica TCS SP8 using a HC PL APO CS2 63×/1.4 NA immersion oil objective. Images were deconvolved using Huygens Professional. Manders' overlap coefficient was calculated using the Coloc2 tool of the FIJI software. Image processing was performed using FIJI. Quantification of KEAP1-positive parasites was done using a Leica DM5500B epifluorescence microscope. Only UIS4-positive parasites were considered. Parasites were counted KEAP1-positive if a clear association between GFP-KEAP1 and UIS4 at the parasite circumference was observed.

Automated live cell imaging was used to determine parasite size and numbers. mCherry- or GFP-expressing parasites were imaged with an INCell Analyzer 2000 automated live cell imaging system (GE Healthcare Life Sciences). InCell Developer Toolbox 1.10.0 software was used to analyze the acquired images. Segmentation was done using the "object" mode in the mCherry or GFP channel, and postprocessing 2 was done to exclude objects smaller than 10 μm^2.

4.10. Measuring NRF2 Activity by Bioluminescence Assay. HuH7-OKD48 cells were infected with *P. berghei* sporozoites expressing mCherry. 5 hpi, cells were detached by Accutase treatment and sorted by FACS into an infected and a noninfected/control population. FACS was performed on a MoFlo Astrios EQ cell sorter (Beckman Coulter). Gates were set to exclude doublets and dead cells as well as debris. Sorted control cells were 100% noninfected while in the infected population 90% +/−2% of the cells were infected. After sorting, cells were seeded in a white 96-well plate (Greiner, 655094) and used for bioluminescence and cell viability assay at 6 hpi. 5000 cells per well were seeded. and 3 technical replicates per experiment were analyzed. Additionally, nontreated and an ASN-treated (1 μM for 6 hours) controls were included. For the purpose of normalization, the number of living cells per well was determined by CellTiter-Fluor Cell Viability Assay (Promega, G6080) according to the manufacturer's instructions. Subsequently, luciferase activity was measured using the Nano-Glo Luciferase Assay System (Promega, N1110) according to the manufacturer's protocol. Cell viability and luciferase assays were performed on the Cytation5 Cell Imaging Multi-Mode Reader (BioTek).

4.11. In Vivo Bioluminescence Imaging of Liver Stage Development. For bioluminescence imaging of liver stage development, 1×10^5 *P. berghei* sporozoites of the strain *Pb*mCherry$_{hsp70}$-Luc$_{eef1\alpha}$ were collected from salivary glands of infected *Anopheles stephensi* mosquitoes and injected intravenously into female C57BL/6 WT and *Nrf2*$^{-/-}$ (B6. Nfe2l2tm1Mym; [9]) mice 10 to 12 weeks of age. The *Nrf2*$^{-/-}$ mice were a kind gift of Dr. Stefan Freigang (University of Bern, Switzerland). Two noninfected controls were included in each experiment for background substraction. The belly of all mice involved in the experiment was shaved beforehand. Luciferase activity in all mouse groups was determined by full-body imaging of mice using an NightOWL LB983 In Vivo Imaging System (Berthold Technologies). Infected mice were anaesthetized using isofluorane. Measurements were performed at 30 and 45 hpi. For luciferase quantification, anaesthetized mice were injected with 100 μl of RediJect D-Luciferin (30 mg/ml; Perkin Elmer, 770504) intraperitoneally. Measurements were performed 7 min after injection of the substrate with an integration time of 3 min. Quantitative analysis was performed using the IndiGO software version 2.0.5.0.

5. Statistical Analysis

All experiments were repeated at least three times independently. Total number of experiments and sample size analyzed is indicated in the respective figure legend. Mean and standard deviations are indicated. All experimental conditions were statistically analyzed by either 2-tailed, unpaired Student's *t*-test when comparing two groups only, or one-way ANOVA test when comparing multiple conditions. ANOVA tests were coupled to Tukey's post hoc test to analyze pairwise conditions. GraphPad Prism version 9 was used to perform statistical analysis and to draw graphs.

Data Availability

All relevant data are within the paper. The data that support the findings of this study are available on request from the corresponding author.

Conflicts of Interest

The authors declare no conflict of interests.

Authors' Contributions

AB, JS, RW, NK, RR, and RC conducted the experiments. VH supervised and coordinated the project. AB, JS, RW, NK, RC, and VH analyzed the data. AB, JS, and VH conceived and designed experiments. AB and VH wrote the paper.

Acknowledgments

Dr. Kerry Woods is thanked for critically reading the manuscript. Prof. Takao Iwawaki and Dr. Conrad Weihl are acknowledged for providing the plasmid p(3xARE)TKbasal-hNrf2(1-433)-GL4-F and both p62 plasmids (mCherry-p62 and mCherry-p62-T350A), respectively. The anti-PhosphoSer351-p62 antibody was an appreciated gift of Dr. Yoshinobu Ichimura. We are grateful to Dr. Stefan Freigang for providing the *Nrf2*$^{-/-}$ mice. Dr. Philippe Plattet is thanked for giving access to Cytation5 for luminescence assays. We thank the MIC (Microscopy Imaging Centre) in Bern for providing excellent imaging facilities and technical support. This work was funded by the Swiss National Science Foundation (SNSF) (grant number 310030_182465) to Volker Heussler.

Supplementary Materials

Figure S1: (A) LC3 colocalizes with UIS4 in *P. berghei* infected mouse primary hepatocytes. Mouse primary hepatocytes were isolated and infected with *Pb*mCherry (red). Cells were fixed at 6 hpi and stained with antibodies against LC3B (green) and UIS4 (magenta). Imaging was performed on a confocal laser scanning microscope. Images were deconvolved using Huygens Professional software. Scale bar: 10 μm. (B) Quantification of (A). The Manders' Overlap Coefficient of 20 images was calculated using FIJI. Every parasite analyzed is represented by one dot. The pink dot represents the parasite depicted in (A). (C) Additional representative images of the data displayed in Figure 3 A&B. Primary mouse hepatocytes were infected with *Pb*mCherry parasites (red). 6 hpi, cells were fixed and stained with either anti-UIS4 (magenta; upper panel) or anti-LC3 antibodies (magenta; middle panel) to visualize

the PVM. p62 was stained using an anti-p62 antibody or an antibody specifically recognizing p62 phosphorylated at serine 351. Images were taken at a confocal laser scanning microscope and deconvolved using Huygens Professional. Scale bar: 10 μm. Note that p62 localizes to the PVM and is phosphorylated at S351. (D) P62 at the PVM is phosphorylated at Ser349 in HuH7 cells. HuH7 cells were infected with *Pb*mCherry (red). Cells were fixed at 6 hpi and stained with antibodies against p62 (green) and an antibody specifically recognizing p62 phosphorylated at serine 349 (magenta). The PVM was visualized by transient transfection of BFP-LC3 (cyan; upper panel). DNA was visualized using Dapi (cyan; lower panel). Scale bar: 10 μm. Note that in noninfected cells there is nearly no phosphorylated p62. Figure S2: HuH7 WT cells stably expressing roGFP2 in the cytoplasm were treated with different concentrations of ASN to induce oxidative stress. Single cells were imaged once with excitation 405 nm and once with excitation 488 nm with the same detection range of 500 nm to 550 nm. Signal intensities for both excitation wavelengths were measured using FIJI. The graph depicts the ratio of both signal intensities which each dot representing one single cell. $N = 10$-12 per condition. Graph shows mean and SD. *P*-values were calculated using a one-way ANOVA test followed by Tukey's post hoc test ($^{**}p \leq 0.01$; $^{***}p \leq 0.001$; and $^{****}p \leq 0.0001$). Figure S3: (A) Parasite load in the liver of *Nrf2*$^{-/-}$ mice is not significantly lowered. WT and *Nrf2*$^{-/-}$ mice were injected intravenously with 50'000 *P. berghei* sporozoites constitutively expressing luciferase (*Pb*mCherry$_{hsp70}$-Luc$_{eef1\alpha}$; [29]. At 30 and 45 hpi the mice were anesthetized, injected with luciferin and parasite load in the liver was analyzed using an In Vivo Imaging System (IVIS). The graphs show total photons per second with each dot representing one mouse. $N = 12$ per group out of 3 experiments. Mean and SD are depicted. P-values were determined using a Student's t-test (ns: $p > 0.05$). (B) Primary hepatocytes isolated from WT or *Nrf2*$^{-/-}$ mice were infected with *Pb*mCherry sporozoites. Parasite numbers were evaluated at 6 and 48 hpi using automated high throughput live cell imaging and analysis (InCell Analyzer 2000). The graph shows the relative parasite survival from 6 to 48 hpi compared to the WT situation. Mean and SD of three independent experiments are depicted. $N > 2500$ parasites per cell line and experiment. A Student's *t*-test was used to determine *P*-values (ns: $p > 0.05$). (C) Parasite size at 48 hpi of the experiment described in (B). The graph shows the medians in parasite size of 3 experiments. Mean and SD are depicted. $N > 1000$ parasites per cell line and experiment. *P*-values were determined using a Student's *t* -test (ns: $p > 0.05$). *(Supplementary Materials)*

References

[1] R. Amino, S. Thiberge, B. Martin et al., "Quantitative imaging of *Plasmodium* transmission from mosquito to mammal," *Nature Medicine*, vol. 12, no. 2, pp. 220–224, 2006.

[2] F. Frischknecht, P. Baldacci, B. Martin et al., "Imaging movement of malaria parasites during transmission by anopheles mosquitoes," *Cellular Microbiology*, vol. 6, no. 7, pp. 687–694, 2004.

[3] R. Amino, D. Giovannini, S. Thiberge et al., "Host cell traversal is important for progression of the malaria parasite through the dermis to the liver," *Cell Host & Microbe*, vol. 3, no. 2, pp. 88–96, 2008.

[4] T. Spielmann, G. N. Montagna, L. Hecht, and K. Matuschewski, "Molecular make-up of the *Plasmodium* parasitophorous vacuolar membrane," *International Journal of Medical Microbiology*, vol. 302, no. 4-5, pp. 179–186, 2012.

[5] P. C. Burda, M. Schaffner, G. Kaiser, M. Roques, B. Zuber, and V. T. Heussler, "A *Plasmodium* plasma membrane reporter reveals membrane dynamics by live- cell microscopy," *Scientific Reports*, vol. 7, no. 1, p. 9740, 2017.

[6] A. Sturm, R. Amino, C. van de Sand et al., "Manipulation of host hepatocytes by the malaria parasite for delivery into liver sinusoids," *Science*, vol. 313, no. 5791, pp. 1287–1290, 2006.

[7] C. van de Sand, S. Horstmann, A. Schmidt et al., "The liver stage of Plasmodium berghei inhibits host cell apoptosis," *Molecular Microbiology*, vol. 58, no. 3, pp. 731–742, 2005.

[8] B. N. Chorley, M. R. Campbell, X. Wang et al., "Identification of novel NRF2-regulated genes by ChIP-Seq: influence on retinoid X receptor alpha," *Nucleic Acids Research*, vol. 40, no. 15, pp. 7416–7429, 2012.

[9] K. Itoh, T. Chiba, S. Takahashi et al., "An Nrf2/small Maf heterodimer mediates the induction of phase II detoxifying enzyme genes through antioxidant response elements," *Biochemical and Biophysical Research Communications*, vol. 236, no. 2, pp. 313–322, 1997.

[10] G. Jiang, X. Liang, Y. Huang et al., "p62 promotes proliferation, apoptosis-resistance and invasion of prostate cancer cells through the Keap1/Nrf2/ARE axis," *Oncology Reports*, vol. 43, no. 5, pp. 1547–1557, 2020.

[11] M. Kobayashi and M. Yamamoto, "Molecular mechanisms activating the Nrf2-Keap1 pathway of antioxidant gene regulation," *Antioxidants & Redox Signaling*, vol. 7, no. 3-4, pp. 385–394, 2005.

[12] D. Malhotra, E. Portales-Casamar, A. Singh et al., "Global mapping of binding sites for Nrf2 identifies novel targets in cell survival response through ChIP-Seq profiling and network analysis," *Nucleic Acids Research*, vol. 38, no. 17, pp. 5718–5734, 2010.

[13] A. Afriat, V. Zuzarte-Luís, K. B. Halpern et al., *A spatiotemporally resolved single cell atlas of the Plasmodium liver stage*, bioRxiv, 2021.

[14] A. A. Ruberto, S. P. Maher, A. Vantaux et al., *Single-cell RNA profiling of Plasmodium vivax liver stages reveals parasite- and host- specific transcriptomic signatures and drug targets*, bioRxiv, 2022.

[15] K. Itoh, N. Wakabayashi, Y. Katoh et al., "Keap1 represses nuclear activation of antioxidant responsive elements by Nrf2 through binding to the amino-terminal Neh2 domain," *Genes & Development*, vol. 13, no. 1, pp. 76–86, 1999.

[16] S. B. Cullinan, J. D. Gordan, J. Jin, J. W. Harper, and J. A. Diehl, "The Keap1-BTB protein is an adaptor that bridges Nrf2 to a Cul3-based E3 ligase: oxidative stress sensing by a Cul3-Keap1 ligase," *Molecular and Cellular Biology*, vol. 24, no. 19, pp. 8477–8486, 2004.

[17] M. Furukawa and Y. Xiong, "BTB protein Keap1 targets antioxidant transcription factor Nrf2 for ubiquitination by the Cullin 3-Roc1 ligase," *Molecular and Cellular Biology*, vol. 25, no. 1, pp. 162–171, 2005.

[18] A. Kobayashi, M. I. Kang, H. Okawa et al., "Oxidative stress sensor Keap1 functions as an adaptor for Cul3-based E3 ligase to regulate proteasomal degradation of Nrf2," *Molecular and Cellular Biology*, vol. 24, no. 16, pp. 7130–7139, 2004.

[19] A. T. Dinkova-Kostova, W. D. Holtzclaw, R. N. Cole et al., "Direct evidence that sulfhydryl groups of Keap1 are the sensors regulating induction of phase 2 enzymes that protect against carcinogens and oxidants," *Proceedings of the National Academy of Sciences of the United States of America*, vol. 99, no. 18, pp. 11908–11913, 2002.

[20] A. L. Levonen, A. Landar, A. Ramachandran et al., "Cellular mechanisms of redox cell signalling: role of cysteine modification in controlling antioxidant defences in response to electrophilic lipid oxidation products," *The Biochemical Journal*, vol. 378, no. 2, pp. 373–382, 2004.

[21] H. Motohashi, T. O'Connor, F. Katsuoka, J. D. Engel, and M. Yamamoto, "Integration and diversity of the regulatory network composed of Maf and CNC families of transcription factors," *Gene*, vol. 294, no. 1-2, pp. 1–12, 2002.

[22] I. M. Copple, A. Lister, A. D. Obeng et al., "Physical and functional interaction of sequestosome 1 with Keap1 regulates the Keap1-Nrf2 cell defense pathway," *The Journal of Biological Chemistry*, vol. 285, no. 22, pp. 16782–16788, 2010.

[23] M. Komatsu, H. Kurokawa, S. Waguri et al., "The selective autophagy substrate p62 activates the stress responsive transcription factor Nrf2 through inactivation of Keap1," *Nature Cell Biology*, vol. 12, no. 3, pp. 213–223, 2010.

[24] A. Lau, X. J. Wang, F. Zhao et al., "A noncanonical mechanism of Nrf2 activation by autophagy deficiency: direct interaction between Keap1 and p62," *Molecular and Cellular Biology*, vol. 30, no. 13, pp. 3275–3285, 2010.

[25] Y. Ichimura, S. Waguri, Y. S. Sou et al., "Phosphorylation of p62 activates the Keap1-Nrf2 pathway during selective autophagy," *Molecular Cell*, vol. 51, no. 5, pp. 618–631, 2013.

[26] A. Jain, T. Lamark, E. Sjottem et al., "*p62/SQSTM1* Is a Target Gene for Transcription Factor NRF2 and Creates a Positive Feedback Loop by Inducing Antioxidant Response Element-driven Gene Transcription∗," *The Journal of Biological Chemistry*, vol. 285, no. 29, pp. 22576–22591, 2010.

[27] J. Schmuckli-Maurer, V. Reber, R. Wacker, A. Bindschedler, A. Zakher, and V. T. Heussler, "Inverted recruitment of autophagy proteins to the Plasmodium berghei parasitophorous vacuole membrane," *PLoS One*, vol. 12, no. 8, article e0183797, 2017.

[28] D. Oikawa, R. Akai, M. Tokuda, and T. Iwawaki, "A transgenic mouse model for monitoring oxidative stress," *Scientific Reports*, vol. 2, no. 1, p. 229, 2012.

[29] M. Prado, N. Eickel, M. De Niz et al., "Long-term live imaging reveals cytosolic immune responses of host hepatocytes against Plasmodium infection and parasite escape mechanisms," *Autophagy*, vol. 11, no. 9, pp. 1561–1579, 2015.

[30] C. Thieleke-Matos, M. Lopes da Silva, L. Cabrita-Santos et al., "Host cell autophagy contributes toPlasmodiumliver development," *Cellular Microbiology*, vol. 18, no. 3, pp. 437–450, 2016.

[31] R. Wacker, N. Eickel, J. Schmuckli-Maurer et al., "LC3-association with the parasitophorous vacuole membrane of Plasmodium bergheiliver stages follows a noncanonical autophagy pathway," *Cellular Microbiology*, vol. 19, no. 10, 2017.

[32] A. J. Meyer and T. P. Dick, "Fluorescent protein-based redox probes," *Antioxidants & Redox Signaling*, vol. 13, no. 5, pp. 621–650, 2010.

[33] J. A. Blaho, "Virus infection and apoptosis (issue II) an introduction: cheating death or death as a fact of life?," *International Reviews of Immunology*, vol. 23, no. 1-2, pp. 1–6, 2004.

[34] V. T. Heussler, P. Kuenzi, and S. Rottenberg, "Inhibition of apoptosis by intracellular protozoan parasites," *International Journal for Parasitology*, vol. 31, no. 11, pp. 1166–1176, 2001.

[35] T. Jiang, B. Harder, M. Rojo de la Vega, P. K. Wong, E. Chapman, and D. D. Zhang, "p62 links autophagy and Nrf2 signaling," *Free Radical Biology and Medicine*, vol. 88, Part B, pp. 199–204, 2015.

[36] C. Tonelli, I. I. C. Chio, and D. A. Tuveson, "Transcriptional regulation by Nrf2," *Antioxidants & Redox Signaling*, vol. 29, no. 17, pp. 1727–1745, 2018.

[37] J. Ma, H. Cai, T. Wu et al., "PALB2 interacts with KEAP1 to promote NRF2 nuclear accumulation and function," *Molecular and Cellular Biology*, vol. 32, no. 8, pp. 1506–1517, 2012.

[38] S. C. Lo and M. Hannink, "PGAM5 tethers a ternary complex containing Keap1 and Nrf2 to mitochondria," *Experimental Cell Research*, vol. 314, no. 8, pp. 1789–1803, 2008.

[39] B. E. Hast, D. Goldfarb, K. M. Mulvaney et al., "Proteomic analysis of ubiquitin ligase KEAP1 reveals associated proteins that inhibit NRF2 ubiquitination," *Cancer Research*, vol. 73, no. 7, pp. 2199–2210, 2013.

[40] N. D. Camp, R. G. James, D. W. Dawson et al., "Wilms tumor gene on X chromosome (WTX) inhibits degradation of NRF2 protein through competitive binding to KEAP1 protein," *The Journal of Biological Chemistry*, vol. 287, no. 9, pp. 6539–6550, 2012.

[41] M. Herb and M. Schramm, "Functions of ROS in macrophages and antimicrobial immunity," *Antioxidants (Basel)*, vol. 10, no. 2, 2021.

[42] F. Yarovinsky, "Innate immunity to *Toxoplasma gondii* infection," *Nature Reviews. Immunology*, vol. 14, no. 2, pp. 109–121, 2014.

[43] V. Zuzarte-Luis, J. Mello-Vieira, I. M. Marreiros et al., "Dietary alterations modulate susceptibility to *Plasmodium* infection," *Nature Microbiology*, vol. 2, no. 12, pp. 1600–1607, 2017.

[44] H. S. Kain, E. K. K. Glennon, K. Vijayan et al., "Liver stage malaria infection is controlled by host regulators of lipid peroxidation," *Cell Death and Differentiation*, vol. 27, no. 1, pp. 44–54, 2020.

[45] S. J. Dixon, K. M. Lemberg, M. R. Lamprecht et al., "Ferroptosis: an iron-dependent form of nonapoptotic cell death," *Cell*, vol. 149, no. 5, pp. 1060–1072, 2012.

[46] L. Jiang, N. Kon, T. Li et al., "Ferroptosis as a p53-mediated activity during tumour suppression," *Nature*, vol. 520, no. 7545, pp. 57–62, 2015.

[47] A. Kaushansky, A. S. Ye, L. S. Austin et al., "Suppression of host p53 is critical for Plasmodium liver-stage infection," *Cell Reports*, vol. 3, no. 3, pp. 630–637, 2013.

[48] L. Feng, K. Zhao, L. Sun et al., "SLC7A11 regulated by NRF2 modulates esophageal squamous cell carcinoma radiosensitivity by inhibiting ferroptosis," *Journal of Translational Medicine*, vol. 19, no. 1, p. 367, 2021.

[49] M. Abdalkader, R. Lampinen, K. M. Kanninen, T. M. Malm, and J. R. Liddell, "Targeting Nrf2 to suppress ferroptosis and mitochondrial dysfunction in neurodegeneration," *Frontiers in Neuroscience*, vol. 12, p. 466, 2018.

[50] J. Lu, Y. Zhao, M. Liu, J. Lu, and S. Guan, "Toward improved human health: Nrf2 plays a critical role in regulating ferroptosis," *Food & Function*, vol. 12, no. 20, pp. 9583–9606, 2021.

[51] X. Song and D. Long, "Nrf2 and Ferroptosis: a new research direction for neurodegenerative diseases," *Frontiers in Neuroscience*, vol. 14, p. 267, 2020.

[52] T. Imai, T. Iwawaki, R. Akai et al., "Evaluating experimental cerebral malaria using oxidative stress indicator OKD48 mice," *International Journal for Parasitology*, vol. 44, no. 10, pp. 681–685, 2014.

[53] S. Epiphanio, S. A. Mikolajczak, L. A. Goncalves et al., "Heme oxygenase-1 is an anti-inflammatory host factor that promotes murine Plasmodium liver infection," *Cell Host & Microbe*, vol. 3, no. 5, pp. 331–338, 2008.

[54] A. Herengt, J. Thyrsted, and C. K. Holm, "NRF2 in viral infection," *Antioxidants (Basel)*, vol. 10, no. 9, 2021.

[55] Y. Pang, Z. Zhang, Y. Chen, S. Cao, X. Yang, and H. Jia, "The Nrf2 pathway is required for intracellular replication of toxoplasma gondii in activated macrophages," *Parasite Immunology*, vol. 41, no. 5, article e12621, 2019.

[56] A. C. Vivarini, T. C. Calegari-Silva, A. M. Saliba et al., "Systems approach reveals nuclear factor erythroid 2-related factor 2/protein kinase R crosstalk in human cutaneous Leishmaniasis," *Frontiers in Immunology*, vol. 8, p. 1127, 2017.

[57] M. A. El-Brolosy and D. Y. R. Stainier, "Genetic compensation: a phenomenon in search of mechanisms," *PLoS Genetics*, vol. 13, no. 7, article e1006780, 2017.

[58] K. Chan, R. Lu, J. C. Chang, and Y. W. Kan, "NRF2, a member of the NFE2 family of transcription factors, is not essential for murine erythropoiesis, growth, and development," *Proceedings of the National Academy of Sciences of the United States of America*, vol. 93, no. 24, pp. 13943–13948, 1996.

[59] P. C. Burda, M. A. Roelli, M. Schaffner, S. M. Khan, C. J. Janse, and V. T. Heussler, "A Plasmodium phospholipase is involved in disruption of the liver stage parasitophorous vacuole membrane," *PLoS Pathogens*, vol. 11, no. 3, article e1004760, 2015.

[60] B. Franke-Fayard, H. Trueman, J. Ramesar et al., "A *Plasmodium berghei* reference line that constitutively expresses GFP at a high level throughout the complete life cycle," *Molecular and Biochemical Parasitology*, vol. 137, no. 1, pp. 23–33, 2004.

[61] Y. Lee, T. F. Chou, S. K. Pittman, A. L. Keith, B. Razani, and C. C. Weihl, "Keap1/Cullin3 modulates p62/SQSTM1 activity via UBA domain ubiquitination," *Cell Reports*, vol. 19, no. 1, pp. 188–202, 2017.

[62] L. Niklaus, C. Agop-Nersesian, J. Schmuckli-Maurer, R. Wacker, V. Grunig, and V. T. Heussler, "Deciphering host lysosome-mediated elimination of *Plasmodium berghei* liver stage parasites," *Scientific Reports*, vol. 9, no. 1, p. 7967, 2019.

[63] W. Fan, Z. Tang, D. Chen et al., "Keap1 facilitates p62-mediated ubiquitin aggregate clearance via autophagy," *Autophagy*, vol. 6, no. 5, pp. 614–621, 2010.

[64] G. B. Waypa, J. D. Marks, R. Guzy et al., "Hypoxia triggers subcellular compartmental redox signaling in vascular smooth muscle cells," *Circulation Research*, vol. 106, no. 3, pp. 526–535, 2010.

[65] C. Agop-Nersesian, M. De Niz, L. Niklaus, M. Prado, N. Eickel, and V. T. Heussler, "Shedding of host autophagic proteins from the parasitophorous vacuolar membrane of *Plasmodium berghei*," *Scientific Reports*, vol. 7, no. 1, p. 2191, 2017.

[66] F. A. Ran, P. D. Hsu, C. Y. Lin et al., "Double nicking by RNA-guided CRISPR Cas9 for enhanced genome editing specificity," *Cell*, vol. 154, no. 6, pp. 1380–1389, 2013.

[67] L. Cong, F. A. Ran, D. Cox et al., "Multiplex genome engineering using CRISPR/Cas systems," *Science*, vol. 339, no. 6121, pp. 819–823, 2013.

[68] F. A. Ran, P. D. Hsu, J. Wright, V. Agarwala, D. A. Scott, and F. Zhang, "Genome engineering using the CRISPR-Cas9 system," *Nature Protocols*, vol. 8, no. 11, pp. 2281–2308, 2013.

[69] N. E. Sanjana, O. Shalem, and F. Zhang, "Improved vectors and genome-wide libraries for CRISPR screening," *Nature Methods*, vol. 11, no. 8, pp. 783-784, 2014.

[70] P. Bialk, Y. Wang, K. Banas, and E. B. Kmiec, "Functional gene knockout of *NRF2* increases chemosensitivity of human lung cancer A549 cells *in vitro* and in a xenograft mouse model," *Molecular Therapy Oncolytics*, vol. 11, pp. 75–89, 2018.